# Adenosine monophosphate is elevated in the bronchoalveolar lavage fluid of mice with acute respiratory toxicity induced by nanoparticles with high surface hydrophobicity

Dailey, Lea Ann; Hernández-Prieto, Raquel; Casas-Ferreira, Ana Maria; Jones, Marie-Christine; Riffo-Vasquez, Yanira; Rodríguez-Gonzalo, Encarnación; Spina, Domenico; Jones, Stuart A; Smith, Norman W; Forbes, Ben; Page, Clive; Legido-Quigley, Cristina

*DOI:*
10.3109/17435390.2014.894150

*Document Version*
Early version, also known as pre-print

*Citation for published version (Harvard):*
Dailey, LA, Hernández-Prieto, R, Casas-Ferreira, AM, Jones, M-C, Riffo-Vasquez, Y, Rodríguez-Gonzalo, E, Spina, D, Jones, SA, Smith, NW, Forbes, B, Page, C & Legido-Quigley, C 2015, 'Adenosine monophosphate is elevated in the bronchoalveolar lavage fluid of mice with acute respiratory toxicity induced by nanoparticles with high surface hydrophobicity', *Nanotoxicology*, vol. 9, no. 1, pp. 106-115.
https://doi.org/10.3109/17435390.2014.894150

# Elevated adenosine monophosphate in bronchoalveolar lavage fluid correlates with acute respiratory toxicity induced by nanoparticles of increasing surface hydrophobicity

*Lea Ann Dailey[a,f]*, Raquel Hernández-Prieto[a,d], Ana Maria Casas-Ferreira[d], Marie-Christine Jones[e], Yanira Riffo-Vasquez[a,c], Encarnación Rodríguez-Gonzalo[d], Domenico Spina[a,c], Stuart A. Jones[a], Norman W. Smith[b], Ben Forbes[a], Clive Page[a,c], Cristina Legido-Quigley[a]**

[a]Institute of Pharmaceutical Science, King's College London, 150 Stamford Street, SE1 9NH London, UK

[b]Division of Environmental and Analytical Science, King's College London, 150 Stamford Street, SE1 9NH London, UK

[c]Sackler Institute of Pulmonary Pharmacology, King's College London, 150 Stamford Street, London SE1 9NH London, UK

[d]Department of Analytical Chemistry, Nutrition and Food Science, University of Salamanca. Spain.

[e]Pharmacy, Pharmacology, Therapeutics section, School of Clinical and Experimental Medicine, University of Birmingham, Birmingham, UK, B15 2TT.

[f]MRC-PHE Centre for Environment and Health

*Corresponding authors

Lea Ann Dailey

[a]Institute of Pharmaceutical Science, King's College London, 150 Stamford Street, SE1 9NH London, UK

Telephone: +44 207 848 4780

Email: lea_ann.dailey@kcl.ac.uk

Crisitina Legido-Quigley

[a]Institute of Pharmaceutical Science, King's College London, 150 Stamford Street, SE1 9NH London, UK

Telephone: +44 207 848 4722

Email: cristina.legido_quigley@kcl.ac.uk

**Abstract**

Pulmonary exposure to certain nanoparticles can induce lung inflammation and tissue damage characterized by neutrophil influx,elevated cytokine and total protein levels in bronchoalveolar lavage (BAL) fluid. In this study, measures of acute lung toxicity were assessed following single-dose intratracheal administration of nanoparticles with varying surface hydrophobicity (i.e. pegylated lipid nanocapsules, polyvinyl acetate nanoparticles and polystyrene beads; listed in order of increasing hydrophobicity). BAL fluid was collected from mice exposed to nanoparticles at a surface area dose of 220 $cm^2$ and metabolite fingerprints were acquired via ultra pressure liquid chromatography-mass spectrometry-based metabolomics. Multivariate analysis of the resultant small molecule fingerprints revealed clear discrimination between the vehicle control and polystyrene beads ($p<0.05$), as well as between nanoparticles of low and high surface hydrophobicity ($p<0.0001$). Further investigation of the metabolic fingerprints revealed that adenosine monophosphate (AMP) concentration in BAL correlated with neutrophilia ($p<0.01$), CXCL1 levels ($p<0.05$) and nanoparticle surface hydrophobicity ($p<0.001$). Our results suggest that extracellular AMP is an intermediary metabolite involved in adenine nucleotide-regulated neutrophilic inflammation and could potentially be used to monitor nanoparticle-induced responses in the lung following pulmonary administration.

***Key words:*** Metabolomics, nanoparticles, lung, hydrophobicity, broncho-alveolar lavage (BAL), inflammation, AMP

## Introduction

When the lungs are exposed, either acutely or chronically, to nanosized materials inflammation and tissue damage can ensue. The nature of the lung response is dependent on the type of material and the dose (Maynard et al. 2011). According to some classifications, nanomaterials may be divided into high and low toxicity materials based on their dose-response in the lungs (Fadeel et al. 2012; Aitken et al. 2009). High toxicity nanoparticles, which induce high levels of inflammation at low doses are generally composed of highly reactive materials, e.g. materials with significant positive or negative surface charge or materials that become toxic upon intracellular processing (Cho et al. 2012). In contrast, low toxicity nanomaterials (e.g. titanium dioxide, gold, silver, and polystyrene) tend to present a much more inert surface, hence they require much higher exposure doses to induce pulmonary inflammation (Duffin et al. 2007; Donaldson et al. 2008). This response to low toxicity nanoparticles is attributed primarily to the high material burden within a given tissue rather than nanomaterial reactivity (Maynard et al. 2011).

The majority of research investigating adverse effects of low toxicity nanomaterials has been conducted using rigid, crystalline, insoluble materials. There has been less research on the response of the respiratory system to the administration of organic nanomaterials (Dailey et al. 2006; Nassimi et al. 2009; Harush-Frenkel et al. 2010; Liu et al., 2009; Beyerle et al. 2011), sometimes referred to as soft nanomaterials (Nalwa, 2009). Organic nanomaterials are increasingly being developed as inhaled nanomedicines or components of aerosol-based consumer products, e.g. hairsprays, cleaning products, and include nanoconstructs such as liquid crystals, proteins, nucleic acids, polymers, surfactants, micelles, or emulsions (Nalwa, 2009). These have very different physicochemical properties compared to rigid crystalline nanoparticles

and typically present an amorphous, more flexible surface that may be highly hydrated (Moghimi & Szebeni 2003; Lorusso et al. 2007; Maynard et al. 2011; Dailey, 2009). Hence, it is important to evaluate how the respiratory system responds to the physicochemistry presented by organic nanomaterials, especially when these are biopersistent.

Surface hydrophobicity is one feature of many organic nanoparticles and has been implicated as a defining factor in how the lungs respond to their administration (Maynard et al. 2011; Beyerle et al. 2011). In this study, hydrophobic interaction chromatography (HIC) (Carstensen et al. 1991) was used to characterize five organic nanomaterials with increasing surface hydrophobicity. The nanomaterials included two different lipid nanocapsule (LNC) formulations, two types of polyvinyl acetate (PVAc) nanoparticles, and commercially available polystyrene beads as a control material to benchmark to the literature. Nanoparticles were administered intratracheally (i.t.) to mice. Bronchoalveolar lavage (BAL) fluid was collected at 24 h and evaluated for markers of inflammation and tissue damage. Neutrophil counts and cytokine levels in BAL confirmed that the nanoparticles induced an inflammatory response linked to increasing surface hydrophobicity, with responses similar to those reported for known inert nanomaterials (Dailey et al. 2006; Duffin et al. 2007; Brown et al. 2001).

The primary aim and scope of this study was then to apply non-targeted metabolomics to assess whether nanoparticle-induced lung toxicity yields informative metabolite profiles in BAL fluid or generates putative markers of nanoparticle-induced toxicity. In metabolomics research, non-targeted investigations are conventionally performed in a phase one study to screen for differences in metabolite levels that indicate perturbations in normal metabolic pathways. The strength of this approach is that it is non-biased towards any particular outcome (i.e. non-hypothesis driven) and may therefore identify putative markers of both known and previously

undiscovered metabolic pathways. Once metabolites of interest have been identified, targeted phase two studies are then designed to investigate specific pathways of interest, evaluate multiple compartments or perform longitudinal studies. In this non-targeted, metabolomics study, it was hypothesized that BAL fluid from vehicle control animals would differ significantly in metabolite profile compared to that of animals exposed to nanoparticles. Further, it was postulated that specific metabolites may be identified which correlate with the acute respiratory toxicity induced by nanoparticles of increasing surface hydrophobicity.

## Methods

**Polymer synthesis.** Two grades of PVAc, high molecular weight (148kDa) and low molecular weight (12.8 kDa), were purchased from Sigma Aldrich, UK. The 148 kDa PVAc was subjected to direct saponification according to the method described by Chana and colleagues (Chana et al. 2008) producing a modified PVAc polymer with 17 mol% hydroxyl groups and 83 mol% residual acetate groups (PVAc80). The 12.8 kDa PVAc polymer was subjected to direct saponification under different reaction conditions to produce a PVAc polymer with 34 mol% hydroxyl groups and 66% residual acetate groups (PVAc60) (Chana et al. 2008). Polymer purity and degree of hydrolysis were verified by NMR analysis prior to use. Poly vinyl alcohol (PVA; 8-12 kDa; 80 mol% hydroxyl; 20 mol% acetate groups) was used a stabiliser in nanoparticle manufacture and was purchased from Sigma Aldrich, UK.

**Manufacture of PVAc nanoparticles.** PVAc60 nanoparticles were prepared according to a method by Chana et al. (Chana et al. 2008) by injecting a solution of 5% w/v PVAc60 dissolved in 2:1 methanol:water into a 0.33 % w/v aqueous solution of the stabiliser, PVA, whilst stirring at 3500 rpm. PVAc80 nanoparticles were prepared by injecting a solution of 1% w/v PVAc80

dissolved in 2:1 methanol:water into a 0.33 % w/v aqueous solution of the stabiliser, PVA, whilst stirring at 3500 rpm. Following 30 min constant stirring at 4000 rpm and solvent evaporation overnight (~100 rpm), the nanosuspensions were dialysed against water (72 h) to remove excess PVA and subsequently concentrated to the desired final concentration using ultrafiltration centrifuge tubes (Millipore, UK; 100 kDa MWCO). Residual PVA was < 0.4-0.5 mg/mL. Particles were stored at 4°C and were used within one week of preparation.

**Manufacture of LNCs:**

LNCs were manufactured using a phase-inversion temperature method (Heurtault et al. 2003). LNCs with a diameter of ~50 nm (LNC50) were prepared by generating a coarse emulsion of 17% w/v Labrafac® WL1349 (Gattefosse, Saint-Priest, France), 17.5% w/v Solutol® HS15 (BASF, Ludwigshafen, Germany), 1.75% w/v Lipoid® S75-3 (Lipoid GmbH, Ludwigshafen, Germany) and 3% w/w NaCl in purified water. This emulsion was then submitted to repeated heating cooling cycles (85°-60°-85°-60°-85° C), before cooling to 72° C, at which point ice-cold water was added. Excess stabilizer (Solutol® HS15) was removed from the suspension by dialysis (72 h) against water containing BioBeads® (BioRad, Hertfordshire, UK) and subsequent concentration using ultrafiltration centrifuge tubes (Millipore, UK; 100 kDa MWCO). Residual Solutol HS 15 content was determined to be < 0.5 mg/mL. LNC with a diameter of ~150 nm (LNC150) were prepared and purified using the same method, except that the relative concentrations of the three main coarse emulsion components were: 25% w/v Labrafac WL1349, 8.5% w/v Solutol® HS15, 1.75% w/v Lipoid S75-3 (Lipoid GmbH, Ludwigshafen, Germany) and 3% w/w NaCl in purified water. Particles were stored at 4°C and were used within one week of preparation.

**Polystyrene nanoparticles.** Unmodified polystyrene nanoparticles with a diameter of 50 nm (PS50; 2.62% m/v) were used as a control and were purchased from Polysciences (Eppelheim, Baden-Württemberg, Germany).

**Nanoparticle size and surface charge.** Particle size and zeta potential were determined using a Zetasizer Nano ZS (Malvern, Worcesterchire, UK). Particle suspensions were diluted in the test medium (purified water, 6.3 mM sodium chloride or Hank's buffered saline solution containing 10% fetal bovine serum) prior to measurement and the analysis parameters (viscosity, temperature, refractive index) were adjusted to match the medium and sample type used for analysis.

**Nanoparticle hydrophobicity:**

Surface hydrophobicity of nanoparticle suspensions (n=3 three individual batches) was assessed using HIC (Carstensen et al. 1991). Briefly, 250 µL nanoparticle suspension was prepared in phosphate-buffered saline (PBS) and eluted through three different HiTrap™ substituted sepharose hydrophobic interaction columns: Butyl FF, Phenyl FF (high substitution) and Octyl FF (GE Healthcare Life Sciences, Little Chalfont, UK). Fractions of 1 mL elutant were collected and analyzed for particle content via turbidity measurement (Lambda 35; Perkin-Elmer, Cambridge, UK; λ=450 nm). The column-bound particle fraction was subsequently eluted from the column using 0.1% Triton X-100 and turbidity measured. Absorbance values were plotted against elution volumes and two area under the curve (AUC) values were calculated using Origin™ software. The percentage particle retention in each of the three columns was defined as:

$$(1) \qquad \%\ \text{Column retention (\%R)} = \left(\frac{\text{AUC } TritonX}{\text{AUC } PBS + \text{AUC } TritonX}\right) * 100$$

The HIC index value was calculated according to Equation (2):

$$(2)\quad \text{HIC Index} = \frac{(\%R_{butyl}) + (\%R_{phenyl}) + (\%R_{octyl})}{300\%}$$

In the denominator, the 300% value represents the theoretical case of 100% retention on each column ideally achieved by a particle with maximum hydrophobicity. HIC index analysis was performed using a one way ANOVA comparison with a post-hoc Tukey test. $p<0.05$ was considered to be statistically significant.

**In vivo studies:**

Male BALBc mice (6–8 weeks old, ~22 g; Charles River, UK) were used for *in vivo* pulmonary administration. All experiments were in accordance with the U.K. Home Office regulations and approved by the local ethics committee. Animals were divided in six groups (n=5-7) for treatment with either the vehicle control (5% dextrose; DEX) or nanoparticle suspensions. Dosing was spread across four different dates, with vehicle controls (1-2 animals) dosed at every session and 2-4 animals from different nanoparticle groups treated on a rotational basis. A theoretical nanoparticle surface area dose of 220 $cm^2$ per instillation was chosen for study as this has been shown to induce a moderate inflammation in selected literature reports (Donaldson et al. 2000; Duffin et al. 2007). Particle surface area doses were calculated from the hydrodynamic diameter of the particles, assuming a density of ca. 1 $g/cm^3$ for PVAc nanoparticles and 0.96 $g/cm^3$ for LNC (estimated from the density of the oil which is the main constituent), and equated to ~200 μg nanoparticles per lung for the smaller LNC50 and PS systems and ~500 μg nanoparticles per lung for the larger LNC150, PVAc60, and PVAc80 systems. All suspensions were prepared in dextrose 5% w/v to ensure isotonicity and colloidal stability and a 5% w/v dextrose solution was used as the vehicle control for all experiments.

Prior to i.t. dosing, animals were anaesthetized by inhaled isoflurane (1-3%) and maintained with an intraperitoneal injection of 100 mg/kg ketamine mixed with 20 mg/kg xylazine in 0.1 mL saline. This combination of tranquilizer/dissociative yielded a moderate level of anesthesia for 15-20 minutes, as assessed by paw pinch withdrawal reflex. Mice were suspended at a 45° angle by their upper incisors and nanosuspensions (50μL) were administered as a coarse aerosol into the lungs using a Penn Century Microsprayer® aerosolizer (Penn-Century Inc. Wyndmoor, PA, USA). Animals were kept warm post-treatment with a heat lamp, then returned to their cages when ambulatory (<15 min). This administration method was chosen as it has been shown to achieve a more homogenous distribution of liquids into the lungs compared with conventional bolus i.t. instillation techniques (Bivas-Benita et al. 2005).

**Assessment of pulmonary inflammation in BAL:**

Mice were euthanized via terminal anesthesia with urethane (2 mg/g i.p., Sigma Chemical Co.) 24 h after nanoparticle administration and a cannula was inserted into the exposed trachea. The lungs were lavaged with three aliquots (0.5 mL) of sterile saline that was recovered through the cannula. The total number of cells in the cellular fraction of the lavage was counted with a Neubauer haemocytometer (Fisher Scientific, Loughborough, UK). Differential cell counts were performed using cytospin preparations (i.e. 100 μL BAL cellular fraction centrifuged at 300 g for 1 min using a Shandon Cytospin 2 (Shandon Southern Instruments, Sewickley, PA, USA) at room temperature). Cells were stained with Diffquick® (DADE Behring, Marburg, Germany) and a total of 200 cells were counted to determine the proportion of neutrophils, eosinophils and mononuclear cells using standard morphological criteria. Eosinophils were not observed in any sample and are not reported. It was assumed that at the time point studied, the mononuclear cell population consisted primarily of resident alveolar macrophages and therefore lymphocyte

numbers were not investigated. Cytokines present in the BAL supernatant were quantified using a murine 7-plex pro-inflammatory cytokine assay (MSD®96-Well Multi-Spot Cytokine Assay; Meso-Scale Discovery, Gainsborough, MD, USA) coupled with an MSD reader, which measures cytokine content via electrochemiluminesce. Of the seven cytokines analyzed (IFN-γ, IL-1β, IL-6, IL-10, IL-12p70, CXCL1 (KC/GRO/CINC), and TNF-α), IL-10 and IL-12p70 were below detectable limits and were therefore excluded from the study. As a measure of tissue integrity, total protein levels in BAL were quantified using a Quick Start™ Bradford Protein Assay (Bio-Rad, Hemel Hempstead, UK) according to manufacturer's instructions. A two-sided Mann-Whitney test was used for the comparison of BAL neutrophil counts, cytokine and protein levels in all samples exposed to nanoparticles compared to the vehicle control (5% dextrose). $p<0.05$ was considered to be statistically significant.

**Sample preparation and UPLC-Q-ToF analysis:**

Extra pure formic acid and LC-MS grade acetonitrile (ACN) and water were purchased from Fluka (Sigma-Adrich). Aliquots (400 µL) of BAL fluid samples (DEX, n=6; LNC50, n=7; LNC150, n=6; PVAc60, n=5; PVAc80, n=7; and PS, n=7) were transferred to clean tubes and evaporated to dryness at 100°C. Samples were reconstituted in 100 µL of 50:50 (v:v) purified water containing 0.1% formic acid and ACN containing 0.1% formic acid. Samples were vortex mixed for 1 min at room temperature. Quality control samples (n=5) consisted of samples without a pre-concentration step. These were used to verify retention time and mass during the duration of the analytical run (Whiley et al. 2012). Samples were run on a Waters Acquity coupled to a Waters Xevo QTOF-MS. The UPLC was performed on a Waters ACQUITY UPLC™ system, equipped with binary solvent delivery manager, sample manager and quadrupole time of flight mass spectrometer. Parameters were as listed: chromatographic column

(Garcia-Perez et al. 2010) UPLC-BEH C18, 2.1×100mm (Waters Corporation, USA); mobile phase A: $H_2O$ (0.1% formic acid) and B: ACN (0.1% formic acid); gradient analysis: 90% A and 10% B isocratic for 0–5, 5–20 min gradient to 100% B, 20–25 min isocratic 100% B; flow rate: 0.5mL/min; pressure circa 9000 psi. The MS was operated in the positive ion mode with a capillary voltage of 2.7 kV and a cone voltage of 50 V. The desolvation gas flow was 490 L/h at a temperature of 300°C and the cone gas flow was 10L/h. A source temperature of 100°C was used. All analyses were acquired using the lock spray to ensure accuracy and reproducibility; leucine enkephalin was used as lock mass (m/z 556.2771 Da) at a concentration of 200 ng/mL and a flow rate of 10μL/min. Data were collected in the centroid mode with a lock spray frequency of 11s over the mass range m/z 50–850 with an acquisition time of 250 ms, inter-scan delay of 50 ms. The chromatograms were obtained by injecting 4 μL. Sample sequences were assembled in blocks with blanks every seven injections to monitor for hydrophobic compound carry-over and QC samples were run to ensure analytical reproducibility. Identification of adenosine monophosphate (AMP) was made by first searching databases and then confirmation with MS-MS analyses of two AMP standard compounds (AMP 5' and 3' standards; Sigma-Aldrich, UK).

**UPLC-Q-ToF data analysis:**

UPLC-Q-ToF data were analyzed using Mass Lynx version 4.1, published by Waters Corporation, Massachusetts, USA, and exported to SIMCA-P™ software version 11.5, published by Umetrics AB, Umeå, Sweden. Data comprised 38 BAL samples, seven blanks and 4,753 variables per chromatogram (each variable was a retention time and m/z). Models were created by normalizing to total chromatogram area and scaling variables to *pareto* in all principal component analyses (PCA), orthogonal partial least squares discriminant analyses (OPLS-DA)

and partial least squares (PLS) analyses. PCA was used to assess quality controls and identify outliers in the groups. PLS detects the variation in the fingerprint data as a whole (x-block) and compares it with variation patterns in the metadata (e.g. discrimination, hydrophobicity, neutrophilia or cytokine levels; y-block). PLS divides the analysis into two parts: one part models the covariation between the fingerprint patterns ($R^2X\%$ is the percentage correlation of the metabolite fingerprints or goodness-of-fit) and the second part models correlation to metadata ($R^2Y\%$). The $Q^2$ (%) or goodness-of-prediction value expressed the prediction power of the model and is the output of a seven-fold cross-validation. Two to three components were calculated for each model. Models were cross-validated independently by 100 fold scrambling and a CV-ANOVA test. Only features that showed high correlation to either treatment group were considered for identification and semi-quantification.

Metabolite identification was achieved by database searching of in-house libraries and the Human Metabolome Database (HMDB; now containing 40,000 metabolite entries) for standard compounds and their molecular fragmentation pattern (Whiley et al. 2012; Xiayan & Legido-Quigley 2008). A two-sided Mann Whitney test was used to assess significance of AMP measurements for all samples exposed to nanoparticles compared to the vehicle control.

## Results

### Manufacture of organic nanoparticles with low to high surface hydrophobicity

Two discrete size classes of nanoparticles (~50 and 150 nm) were included in the study (Table 1). The sizes were dictated by the chemical composition and the manufacturing techniques used to produce the nanoparticles. The nanoparticles studied did not exhibit a pronounced surface charge and all nanoparticles were physically stable in purified water for up to four weeks.

LNC50, LNC150 and PVAc60 retained their original size in Hank's buffered saline (HBSS) at 37°C for over 24 h, but PVA80 and PS50 aggregated immediately upon addition to HBSS (Table 1).

The surface hydrophobicity of the nanoparticles was quantified using a HIC index scale (zero = hydrophilic, 1.00 = hydrophobic). The nanoparticles studied spanned the upper 50% of the HIC index scale, ~0.60-0.96 (Figure 1). PS beads exhibited a nearly maximal hydrophobicity (0.96 ± 0.03) and therefore served as an excellent reference material. The other nanoparticles used in the study exhibited a rank order of LNC50 < LNC150 < PVAc60 < PVAc80. Statistical analysis of the HIC values revealed two major groupings, low surface hydrophobicity particles (LNC50, LNC150 and PVAc60) and high surface hydrophobicity particles (PVAc80 and PS).

**Pulmonary toxicity of high surface hydrophobicity nanoparticles**

Neutrophilia and elevated pro-inflammatory cytokine levels were observed at significant levels in BAL for the two high hydrophobicity nanoparticle treatments, PVAc80 and PS (Figure 2a,b,d). The moderate inflammation induced in response to PS nanoparticles correlated well with benchmark studies (Dailey et al. 2006; Donaldson et al. 2000; Duffin et al. 2007). Total protein levels in BAL from nanoparticle treatment groups were not significantly different from the dextrose vehicle control, which may have resulted from the high variability in the vehicle control group. Trends in the data suggest that high hydrophobicity nanoparticle treatment, especially PS exposure, generally resulted in higher BAL protein levels indicative of possible tissue damage.

As noted above a high variability in both the inflammatory profile and BAL total protein content of the vehicle control (5% dextrose) was observed. Comparisons with untreated controls and animals administered 0.9% saline vehicle via an oral aspiration technique (Figure S1) provided evidence that the higher variability in the data may be linked to Microsprayer®

administration. Careful analysis showed that variability occurred randomly and potential outliers could not be correlated with factors such as animal batch, date of experiment or experience of the operator with the Microsprayer® administration technique. A further rationale for including putative outliers in the study was that it was of interest to examine whether the fingerprints of putative outliers showed metabolite patterns indicative of toxicity (i.e. similar to positive control profiles).

**Nanoparticle treatment results in significant differences in BAL metabolite fingerprints**

In this study, a total of 38 BAL fluid samples from the six treatment groups (vehicle control, nanoparticles, and quality control samples) were investigated. The fingerprints acquired consisted of chromatograms from which 4753 molecular features were extracted. In a preliminary analysis using PCA, quality controls were superimposable verifying analytical reproducibility. OPLS-DA was used to compare the fingerprint profiles of vehicle and PS-treated groups (Figure 3), which acted as negative and positive controls, respectively (Dailey et al. 2006; Duffin et al. 2007; Brown et al. 2001). The analysis discriminated between PS nanoparticle treatment and the vehicle control ($p = 0.041$), indicating that different metabolites dominated the fingerprints of lungs exposed to nanoparticles compared to those that were not. Five molecule masses (m/z 331.20, 284.95, 188.12, 182.18 and 174.10 Da) were identified from the model as unknown metabolites having the highest correlation (0.98 to 0.78) with PS exposure (elevated concentrations found in PS treated group compared to vehicle control). These five molecules did not correspond to any of the known accurate masses in metabolite databases and could not be identified within the scope of this study.

OPLS-DA was also used to compare the BAL fingerprint profiles of animals exposed to low hydrophobicity (LNC50, LNC150 and PVAc60) versus high hydrophobicity (PVAc80 and PS)

nanoparticles (Figure 4). The analysis discriminated between the two HIC-index groupings ($p<0.0001$). Interestingly, all five unknown metabolites associated with PS NP exposure (m/z 331.20, 284.95, 188.12, 182.18and 174.10 Da) were positively correlated in the high versus low HIC comparison model (correlation = 0.83 to 0.50; Figure 4) suggesting that these molecules may be interesting candidates to take forward into targeted,studies of biomarkers for high hydrophobicity nanoparticle exposure.

Partial least squares (PLS) analysis was performed to analyze the incremental relationship between nanoparticle hydrophobicity, inflammatory outcomes and the BAL fingerprints. Total protein levels in BAL were excluded from PLS analysis due to their lack of significance between groups. Table 2 lists the PLS analysis metrics for covariance of fingerprint data and nanoparticle HIC index score, neutrophil counts or BAL CXCL1 concentration, while Figure 5 depicts the PLS score plot correlating to HIC index score. A substantial correlation between metabolite fingerprints and measures of lung inflammation (neutrophils and CXCL1) was indicated by the $Q^2$ values of 65 and 68%, respectively. The model for covariance between metabolite fingerprints and nanoparticle hydrophobicity showed a similar predictive $Q^2$ value of 66%, indicative of the relationship between increasing nanoparticle hydrophobicity, lung inflammation and metabolite fingerprint models.

**Elevated AMP levels correlate with increasing HIC index score**

Analysis of the features that governed the correlation between metabolite fingerprint and HIC index identified a retention and mass of interest. Using standard compounds and fragmentation patterns (Esther et al. 2008b), AMP (m/z 348.06 Da with a main fragment observed at 136.06 Da) was identified as a signature molecule associated with the effects generated in the lungs by nanoparticle of increasing hydrophobicity. The loading plot of the PLS model is provided in the

supplementary information Figure S2, showing the feature identified as AMP driving the trend towards PVAc-80 and PS seen in Figure 5. AMP was measured in all the chromatograms and validation of the molecule identity was performed with the pure compound (supplementary information Figure S3 showing MS-MS AMP identification). Scatter plots depicting paired values of AMP peak areas from the raw data against neutrophil numbers (Figure 6a) and total protein levels (Figure 6b) show that AMP levels are only elevated in BAL samples from high hydrophobicity nanoparticle treatment groups (data summarized in Figure 6c).

**Discussion**

The aims of this study were twofold: 1) to assess the impact of high vs. low nanoparticle surface hydrophobicity on lung toxicity and 2) to apply a non-targeted metabolomics strategy to investigate whether organic nanoparticle exposure would result in significantly differentiated BAL metabolite profiles and to identify putative markers of nanoparticle exposure. Using conventional measures of pulmonary inflammation and tissue damage, it was demonstrated that nanoparticles of different composition exhibiting a high surface hydrophobicity (PVAc80 and PS) were pro-inflammatory and showed possible evidence of tissue damage, while low hydrophobicity nanomaterials (LNC50, LNC150 and PVAc60) induced little to no toxicity according to these parameters. Hydrophobic nanoparticle surface chemistries may induce pulmonary toxicity through more than one mechanism. For example, it has been shown that proteins and opsonins may absorb more favorably onto a hydrophobic surface, promoting recognition, uptake and inflammatory signaling by phagocytic cells (Ruge et al. 2012; Singh & Lillard 2009). A pertinent mechanism in this study may be particle aggregation in physiological fluids resulting in irregular surfaces, which have been associated with higher inflammatory potential than comparable smooth-surface particles (Vaine et al. 2013). Only the nanoparticles in

the high surface hydrophobicity group (PS50 and PVAc80) aggregated in isotonic buffer at 37˚C (Table 1), which may have contributed significantly to their enhanced inflammatory potential and possible tissue damage *in vivo*.

With the impact of nanoparticle surface hydrophobicity established using conventional parameters (aim 1) it was possible to undertake a non-targeted, phase one metabolomics study (aim 2) with the remaining BAL fluid from these study groups. Non-targeted, NMR-based metabolomics screening has been used in a handful of studies to date to analyse intact tissues (lung, liver), as well as biofluids such as urine, serum and BAL from test animals after pulmonary, oral or intravenous exposure to different nanomaterials, including copper oxide, silica and titanium dioxide (Hu et al. 2008; Bu et al. 2010; Lei et al. 2008; Lu et al. 2011). Notably, Hu et al. (2008) examined the pulmonary effects of i.t. administration of high dose silica nanoparticles one week and four months post-exposure. Metabolites identified as highly correlated with silica exposure (both in BAL and lung tissue) were primarily associated with cell membrane damage (elevated cholines and phosphocholine species), as well as elevated levels of hydroxyproline, indicative of the typical fibrosis development associated with silicosis (Hu et al. 2008).

In this study, five unidentified metabolites and AMP were identified as candidate biomarkers of high hydrophobicity nanoparticle exposure. While metabolite identification is of major importance for the design of hypothesis-driven mechanistic studies of toxicity, it must be emphasized that the identification process of unknown molecules from UPLC-MS chromatograms is not trivial, as current databases only hold metabolite mass and fragmentation pattern information on a small fraction of the estimated total number of possible metabolites (Whiley et al. 2012). AMP, on the other hand, was identifiable from databases through its mass,

fragmentation pattern and subsequent validation using a pure standard substance. It was observed that AMP levels in BAL fluid correlated highly with increasing nanoparticle hydrophobicity and acute lung inflammation. This observation was interesting as, in contrast to many putative biomarkers identified in non-targeted metabolomic screens, there is literature evidence to link AMP with known mechanisms of pulmonary toxicity. Figure 7 outlines a hypothetical role for AMP in high hydrophobicity nanoparticle toxicity.

Neutrophilic inflammation is known to be regulated by extracellular purine signaling. Activated neutrophils secrete high quantities of ATP, which acts as a chemotactic agent for further neutrophil recruitment to the site of inflammation (Jacob et al. 2013; Barletta et al. 2012). Elevated extracellular levels of ATP activate the purine receptors, $P_2X$ and $P_2Y$ subtypes, which are expressed across a wide range of cell types in the lung and specifically promote chemotaxis, release of pro-inflammatory cytokines, actin mobilization and enhanced phagocytosis, as well as respiratory burst events in neutrophils (Jacob et al. 2013; Barletta et al. 2012). Because of its potent pro-inflammatory effects, extracellular ATP is rapidly metabolized in the lung lining fluid to ADP, AMP and adenosine at the respiratory epithelial surface. The lung mucosal surface possesses four major classes of enzymes to metabolize ATP to adenosine: ectonucleotidases:ecto-nucleotide pyrophosphatase/phosphodiesterases (E-NPP: ATP → AMP), alkaline phosphatases (AP: ATP → ADP → AMP → adenosine) and ecto-nucleoside triphosphate diphosphohydrolases (E-NTPDases: ATP → AMP) and ecto-5′-nucleotidase (eNT: AMP → adenosine) (Burch & Picher 2006; Robson et al. 2006). Currently, relatively little is known about the direct role of extracellular AMP in inflammation, except as an intermediate metabolite. Adenosine, in contrast, is known to be both a pro-and anti-inflammatory signaling molecule. For example, in neutrophils, adenosine binding to adenosine receptor subtypes $A_1$ and

$A_3$ generally promotes pro-inflammatory responses, while $A_{2A}$ and $A_{2B}$ activation results in anti-inflammatory effects, such as reduction in pro-inflammatory cytokine release, phagocytosis and degranulation (Barletta et al. 2012; Blackburn et al. 2009; Reutershan, 2009). Thus, the regulation of neutrophil response in lung inflammation is controlled both by levels of extracellular signaling molecule levels, as well as differential purine and adenosine receptor expression patterns.

The use of elevated extracellular purine levels as a putative biomarker for disease-induced neutrophilic inflammation has been reported previously. ATP and AMP have been observed to be elevated in BAL fluid samples from cystic fibrosis (CF) patients compared to disease controls (patients with unrelated respiratory disease) as well as in exhaled breath condensate from CF patients vs. healthy controls (Esther et al. 2009; Esther et al. 2008a; Wolak, 2009; Kavitha et al. 2013). Further, a highly significant correlation ($p<0.0001$) between neutrophil counts and increases ATP and AMP was found for all samples irrespective of disease state, supporting the authors' hypothesis that elevated ATP and AMP were a product of the secondary neutrophilic inflammation rather than the primary pathology (Esther et al. 2008a). Interestingly, it was also observed that AMP levels were consistently higher than those of ATP (Esther et al. 2008a), which was speculated by Esther et al. (2008a) to arise from increased metabolism of ATP to AMP by E-NTPDases (present on both neutrophils and epithelial cell surfaces) combined with a lower capacity to convert extracellular AMP to adenosine during inflammation due to a relative lack of 5′-nucleotidase (eNT: AMP → adenosine) on the surface of infiltrating neutrophils.

It should be noted that while the studies described above were able to show a strong direct correlation between neutrophil numbers and AMP levels, as well as ATP levels (Esther et al. 2009; Esther et al. 2008a; Wolak, 2009; Kavitha et al. 2013), our preliminary results do not

reveal a high direct correlation between neutrophil numbers and AMP peak areas in the raw data, even within the high hydrophobicity nanoparticle treatment group (Figure 6a). One important reason for this discrepancy could be explained by the fact that the studies cited above all used optimized protocols to specifically measure ATP and AMP levels in their samples. This is representative of a targeted, phase two approach in the biomarker development pathway. In contrast, the standard analytical protocol used in this study was designed to maximize the detection of the largest number of unknown metabolites, and may not have favored purine detection. In fact, Esther et al. (2008b) report that higher polarity nucleotide species, such as ATP, can be sensitive to low pH mobile phases such as those used in this study (e.g. 0.1% formic acid pH 3-5) and this can have an effect on the limits of detection of the metabolite (Esther et al. 2008b). AMP, a less polar metabolite, is more easily detected in a low pH mobile phase, but may still require further optimization for robust quantification. Thus, it should be emphasized that targeted, phase two studies using optimized analytical conditions to assess concurrent levels of ATP, ADP, AMP and adenosine and longitudinal experimental design are required to shed further light on the overall variation of extracellular purines in nanoparticle-induced acute lung inflammation and tissue damage.

**Conclusions**

This study has demonstrated that hydrophobic nanoparticles induced acute respiratory inflammation when administered into the lungs of mice. The inflammation was characterized by significantly increased neutrophilia, elevated levels of pro-inflammatory cytokines, possible evidence of increased tissue damage and significantly altered metabolite fingerprints in BAL fluid. AMP concentration in BAL was found to correlate with the degree of inflammation 24

hours after administration of the nanoparticles, the time point of peak neutrophilic response. This finding supports the hypothesis that elevated extracellular purines in the lungs may be candidate biomarkers for neutrophilic lung inflammation. It is the first study to our knowledge to demonstrate elevated AMP in response to nanoparticle exposure.

The non-targeted metabolomics screen also yielded five unidentified metabolites that were highly correlated with hydrophobic nanoparticle exposure. The identities of these metabolites will be elucidated in future studies using isolation of molecules and LC-MS techniques combined with NMR analysis. Similar to AMP, the identities of these molecules may shed further light on individual mechanisms of respiratory nanotoxicity and they have the potential to expand meaningfully the range of nanotoxicity biomarkers available to researchers today.

**Acknowledgements**

The authors would like to acknowledge the UK Medical Research Council for funding of the *in vivo* elements of the study and Waters Corporation for support of the Waters Innovation Center at King's College London. R. Hernández-Prieto gratefully acknowledges financial assistance from Ministry of Science and Innovation, Spain (FPI grant and Project CTQ 2011-24075).

**REFERENCES**

Aitken R, Borm P, Donaldson K, Ichihara G, Loft S, Marano F, Maynard A, Oberdörster G, Stamm H, Stone V, Tran L, Wallin H. 2009. Nanoparticles - one word: A multiplicity of different hazards. *Nanotoxicol* 3**:**263-264.

Barletta KE, Ley K, Mehrad B. 2012. Regulation of neutrophil function by adenosine. *Arterioscler Thromb Vasc Biol* 32:856-64.

Beyerle A, Braun A, Banjeree A, Ercal N, Eickelberg O, Kissel T, Stoeger T. 2011. Inflammatory responses to pulmonary application of PEI-based siRNA nanocarriers in mice. *Biomaterials* 32**:**8694-8701.

Bivas-Benita M, Zwier R, Junginger HE, Borchard G. 2005. Non-invasive pulmonary aerosol delivery in mice by the endotracheal route. *Eur J Pharm Biopharm* 61**:**214-8.

Blackburn MR, Vance CO, Morschl E, Wilson CN. 2009. Adenosine receptors and inflammation. *In:* Wilson CN & Mustafa SJ. (ed.) *Adenosine receptors in health and disease*. Heidelberg: Springer-Verlag, pp. 215-269.

Brown DM, Wilson MR, MacNee W, Stone V, Donaldson K. 2001. Size-dependent proinflammatory effects of ultrafine polystyrene particles: a role for surface area and oxidative stress in the enhanced activity of ultrafines. *Toxicol Appl Pharmacol* 175:191-199.

Bu Q, Yan G, Deng P, Peng F, Lin H, Xu Y, Cao Z, Zhou T, Xue A, Wang Y, Cen X, Zhao YL. 2010. NMR-based metabonomic study of the sub-acute toxicity of titanium dioxide nanoparticles in rats after oral administration. *Nanotechnology* 21:125105.

Burch LH & Picher M. 2006. E-NTPDases in human airways: Regulation and relevance for chronic lung diseases. *Purinergic Signal* 2**:**399-408.

Button BM & Button B. 2013. Structure and function of the mucus clearance system of the lung. *Cold Spring Harbor Perspectives in Medicine,* 3: published in advance June 10, 2013, doi: 10.1101/cshperspect.a009720.

Carstensen H, Müller BW, Müller RH. 1991. Adsorption of ethoxylated surfactants on nanoparticles: 1. Characterization by hydrophobic interaction chromatography. *Int J Pharm* 67**:**29-37.

Chana J, Forbes B, Jones SA. 2008. The synthesis of high molecular weight partially hydrolysed poly(vinyl alcohol) grades suitable for nanoparticle fabrication. *J Nanosci Nanotech* 8: 5739-5747.

Cho WS, Duffin R, Thielbeer F, Bradley M, Megson IL, MacNee W, Poland CA, Tran CL, Donaldson K. 2012. Zeta potential and solubility to toxic ions as mechanisms of lung inflammation caused by metal/metal oxide nanoparticles. *Toxicol Sci* 126:469-477.

Dailey, LA. 2009. Considerations for the design of toxicity studies of inhaled nanomedicines. *In:* Sahu SC & Casciano DA. (eds.) *Nanotoxicity. From In vivo and in vitro models to health risks.* Chichester: John Wiley & Sons Ltd, pp. 41-60.

Dailey LA, Jekel N, Fink L, Gessler T, Schmehl T, Wittmar M, Kissel T, Seeger W. 2006. Investigation of the proinflammatory potential of biodegradable nanoparticle drug delivery systems in the lung. *Toxicol Appl Pharmacol* 215:100-108.

Donaldson K, Borm PJA, Oberdörster G, Pinkerton KE, Stone V, Tran CL. 2008. Concordance between in vitro and in vivo dosimetry in the proinflammatory effects of low-toxicity, low-solubility particles: The key role of the proximal alveolar region. *Inhal Toxicol* 20:53-62.

Donaldson K, Stone V, Gilmour PS, Brown DM, MacNee W. 2000. Ultrafine particles: mechanisms of lung injury. *Philosoph Trans Royal Soc London Ser a-Math Phys Eng Sci* 358:2741-2748.

Duffin R, Tran L, Brown D, Stone V, Donaldson K. 2007. Proinflammogenic effects of low-toxicity and metal nanoparticles in vivo and in vitro: Highlighting the role of particle surface area and surface reactivity. *Inhal Toxicol,* 19:849-856.

Esther CR, Alexis NE, Clas ML, Lazarowski ER, Donaldson SH, Rlbeiro CMP, Moore CG, Davis SD, Boucher RC. 2008a. Extracellular purines are biomarkers of neutrophilic airway inflammation. *Eur Resp J* 31:949-956.

Esther CR, Boysen G, Olsen BM, Collins LB, Ghio AJ Swenberg JW, Boucher RC. 2009. Mass spectrometric analysis of biomarkers and dilution markers in exhaled breath condensate reveals elevated purines in asthma and cystic fibrosis. *Am J Physiol Lung Cell Mol Physiol* 296:L987-L993.

Esther CR, Jasin HM, Collins LB, Swenberg JA, Boysen G. 2008b. A mass spectrometric method to simultaneously measure a biomarker and dilution marker in exhaled breath condensate. *Rapid Commun Mass Spectrom* 22:701-5.

Fadeel B, Pietrouitisi A, Shvendova AA. 2012. *Adverse effects of engineered nanomaterials : exposure, toxicology, and impact on human health,* London; Waltham, MA, Elsevier/Academic Press.

Garcia-Perez I, Earll ME, Angulo S, Barbas C, Legido-Quigely C. 2010. Chemometric analysis of urine fingerprints acquired by liquid chromatography-mass spectrometry and capillary electrophoresis: Application to the schistosomiasis mouse model. *Electrophoresis* 31:2349-2355.

Harush-Frenkel O, Bivas-Benita M, Nassar T, Springer C, Sherman Y, Avital A, Altschuler Y, Borlak J, Benita S. 2010. A safety and tolerability study of differently-charged nanoparticles for local pulmonary drug delivery. *Toxicol Appl Pharmacol* 246:83-90.

Heurtault B, Saulnier P, Pech B, Benoit JP, Proust JE. 2003. Interfacial stability of lipid nanocapsules. *Coll Surf B-Biointerfaces* 30:225-235.

Jacob F, Novo CP, Bachert C, Van Crombruggen K. 2013. Purinergic signaling in inflammatory cells: P2 receptor expression, functional effects, and modulation of inflammatory responses. *Purinergic Signal*. published in advance February, 2013, doi: 10.1007/s11302-013-9357-4.

Hu JZ, Rommereim, DNR, Minard KR, Woodstock A, Harrer BJ, Wind RA, Phipps RP, Sime PJ. 2008. Metabolomics in lung inflammation: A high-resolution 1H NMR study of mice exposed to silica dust. *Toxicol Mech Methods* 18:385-398.

Lei RH, Wu CQ, Yang BH, Ma HZ, Shi C, Wang QJ, Wang QX, Yuan Y, Liao MY. 2008. Integrated metabolomic analysis of the nano-sized copper particle-induced hepatotoxicity and nephrotoxicity in rats: A rapid in vivo screening method for nanotoxicity. *Toxicol Appl Pharmacol* 232**:**292-301.

Liu YJ, Ibricevic A, Cohen JA, Cohen JL, Gunsten SP, Frechet JMJ, Walter MJ, Welch MJ, Brody SL. 2009. Impact of hydrogel nanoparticle size and functionalization on in vivo behavior for lung imaging and therapeutics. *Mol Pharm* 6:1891-1902.

Lorusso D, Di Stefano A, Carone V, Fagotti A, Pisconti S, Scambia G. 2007. Pegylated liposomal doxorubicin-related palmar-plantar erythrodysesthesia (‘hand-foot’ syndrome). *Ann. Oncol.,* 18**,** 1159-1164.

Lu XY, Tian Y, Zhao QQ, Jin TT, Xiao S, Fan XH. 2011. Integrated metabonomics analysis of the size-response relationship of silica nanoparticles-induced toxicity in mice. *Nanotechnology,* 22:055101.

Maynard AD, Warheit DB, Philbert MA. 2011. The new toxicology of sophisticated materials: nanotoxicology and beyond. *Toxicol Sci,* 120 Suppl 1**,** S109-29.

Moghimi SM & Szebeni J. 2003. Stealth liposomes and long circulating nanoparticles: critical issues in pharmacokinetics, opsonization and protein-binding properties. *Prog. Lipid Res.,* 42**,** 463-78.

Nalwa HS. 2009. *Soft nanomaterials,* Stevenson Ranch, Calif., American Scientific Publishers.

Nassimi M, Schleh C, Lauenstein HD, Hussein R, Lübbers K, Pohlmann G, Switalla S, Sewald K, Müller M, Krug N, Müller-Goymann CC, Braun A. 2009. Low cytotoxicity of solid lipid nanoparticles in in vitro and ex vivo lung models. *Inhal Toxicol* 21:104-109.

Picher M, Burch LH, Boucher RC. 2004. Metabolism of P2 receptor agonists in human airways - Implications for mucociliary clearance and cystic fibrosis. *J Biol Chem* 279:20234-20241.

Picher M, Burch LH, Hirsh AJ, Spychala J, Boucher RC. 2003. Ecto 5 '-nucleotidase and nonspecific alkaline phosphatase - Two amp-hydrolyzing ectoenzymes with distinct roles in human airways. *J Biol Chem* 278**:**13468-13479.

Reutershan J, Vollmer I, Stark S, Wagner R, Ngamsri KC, Eltzschig HK. 2009. Adenosine and inflammation: CD39 and CD73 are critical mediators of LPS-induced PMN trafficking into the lungs. FASEB J 23: 473-482.

Robson SC, Sevigny J, Zimmermann H. 2006. The E-NTPDase family of ectonucleotidases: Structure function relationships and pathophysiological significance. *Purinergic Signal* 2:409-30.

Ruge CA, Schaefer UF, Herrmann J, Kirch J, Canadas O, Echaide M, Perez-Gil J, Casals C. Müller R, Lehr CM. 2012. The interplay of lung surfactant proteins and lipids assimilates the macrophage clearance of nanoparticles. *Plos One* 7: e40775.

Singh R & Lillard JW. 2009. Nanoparticle-based targeted drug delivery. *Exp Mol Pathol* 86: 215-223.

Vaine CA, Patel MK, Zhu JT, Lee E, Finberg RW, Hayward RC, Kurt-Jones EA. 2013. Tuning innate immune activation by surface texturing of polymer microparticles: The role of shape in inflammasome activation. *J Immunol* 190:3525-3532.

Whiley L, Godzien J, Ruperez FJ, Legido-Quigley C, Barbas C. 2012. In-vial dual extraction for direct LC-MS analysis of plasma for comprehensive and highly reproducible metabolic fingerprinting. *Anal Chem* 84:5992-5999.

Wolak JE, Esther CR, O'Connell TM. 2009. Metabolomic analysis of bronchoalveolar lavage fluid from cystic fibrosis patients. *Biomarkers,* 14**,** 55-60.

Xiayan L & Legido-Quigley C. 2008. Advances in separation science applied to metabonomics. *Electrophoresis* 29:3724-36.

**Figure captions**

**Figure 1.** Quantitative evaluation of nanoparticle surface hydrophobicity expressed as the HIC index score of five nanomaterials. Values represent the mean ± standard deviation of n=3 individual nanoparticle batches. * $p < 0.05$

**Figure 2.** Assessment of pulmonary toxicity 24 h post intratracheal administration of five nanomaterials based on (a) neutrophil counts, (b) total cells, (c) total protein levels and (d) pro-inflammatory cytokine content in BAL fluid (n=5-7 individual animals per group). * $p< 0.05$, ** $p<0.01$.

**Figure 3.** OPLS-DA scores plot of the vehicle control (5% dextrose solution) and positive control (PS nanoparticle exposure) showing group separation ($p = 0.041$).

**Figure 4.** OPLS-DA scores plot of the low hydrophobicity nanoparticle treatment groups (LNC50, LNC150 and PVAc60) and high hydrophobicity nanoparticle treatment groups (PVAc80 and PS) showing group separation (p-value$< 0.0001$).

**Figure 5:** PLS scores plot showing the relationship between individual nanoparticle fingerprints and HIC index values. The figure also shows the direction of an identified metabolite, AMP, which follows the trend of inflammation.

**Figure 6.** Semi-quantitative analysis of AMP levels. (a) AMP(peak area normalized to total fingerprint area) is plotted against paired values for the number of neutrophils in BAL, (b) AMP (peak area normalized to total fingerprint area) is plotted against paired values for the protein content in BAL, (c) AMP (peak area normalized to total fingerprint area) levels from vehicle control, low hydrophobicity and high hydrophobicity nanoparticle treatment groups. *$p<0.05$, ** $p<0.01$, *** $p<0.001$.

**Figure 7.** A summary diagram outlining hypothetical mechanisms which may be involved in observed increased levels of extracellular purines following exposure to high hydrophobicity nanoparticles. The simplified diagrams of extracellular ATP metabolism are based on information contained in (Burch & Picher 2006; Robson et al. 2006, Barletta et al. 2012;

Blackburn et al. 2009). E-NPP = Ecto-nucleotide pyrophosphatase/phosphodiesterases; AP = alkaline phosphatases; E-NTPDase = ecto-nucleoside triphosphate diphosphohydrolases; eNT = ecto-5′-nucleotidase; ADA = adenosine deaminase; ADK = adenosine kinase.

**Table 1.** Composition and physicochemical properties of the five organic nanoparticles studied.

| | **Lipid nanocapsules** | | **Polymeric nanoparticles** | | |
|---|---|---|---|---|---|
| **Abbreviation** | LNC50 | LNC150 | PVAc60 | PVAc80 | PS |
| **Nanoparticle core** | 90% TG | 93% TG | 99% PVAc60 | 96% PVAc80 | Polystyrene |
| **Nanoparticle stabilizer** | 0.3% PEG-HS 9.3% PC | 0.2% PEG-HS 6.5% PC | 0.8% PVA | 3.8% PVA | Undisclosed |
| **Diameter (nm)** | 40 ± 3 | 143 ± 2 | 160 ± 7 | 165 ± 7 | 54 ± 4 |
| **PDI** | 0.14 ± 0.02 | 0.32 ± 0.42 | 0.13 ± 0.03 | 0.08 ± 0.03 | 0.04 ± 0.02 |
| **ζ (mV)** | -7 ± 4 | -4 ±1 | -3 ± 1 | -4 ± 1 | -25 ± 5 |
| **Stability in $H_2O$ (4°C)** | > 4 weeks | > 4 weeks | > 4 weeks | > 4 weeks | > 4 weeks |
| **Stability in HBSS (37°C)** | >24 h | >24 h | >24 | Immediate aggregation | Immediate aggregation |

*Table abbreviations: PEG-HS= polyethylene glycol$_{660a}$-(15)-hydroxystearate; PC=soy lecithin; TG= medium chain triglycerides; PVA= polyvinyl alcohol; PVAc= polyvinyl acetate; PDI= polydispersity index; ζ= zeta potential*

**Table 2.**PLS analyses to assess correlations between BAL small molecule fingerprints and nanoparticle hydrophobicity (HIC index), neutrophil count or BAL CXCL1 concentration. The $R^2X$, $R^2Y$ and $Q^2$ values are provided for each model in percentage.

| | **HIC Index** | **Neutrophils** | **CXCL1** |
|---|---|---|---|
| **$R^2X$ (%)** | 28 | 28 | 29 |
| **$R^2Y$ (%)** | 98 | 97 | 98 |
| **$Q^2$ (%)** | 66 | 65 | 68 |
| **P-value** | 0.001 | 0.01 | 0.04 |

Figure 1

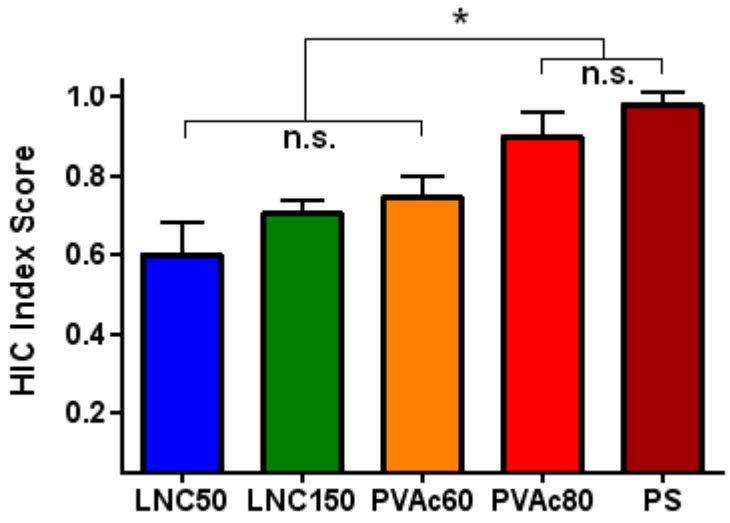
*
n.s.
n.s.
HIC Index Score
1.0
0.8
0.6
0.4
0.2
LNC50
LNC150
PVAc60
PVAc80
PS

Figure 2

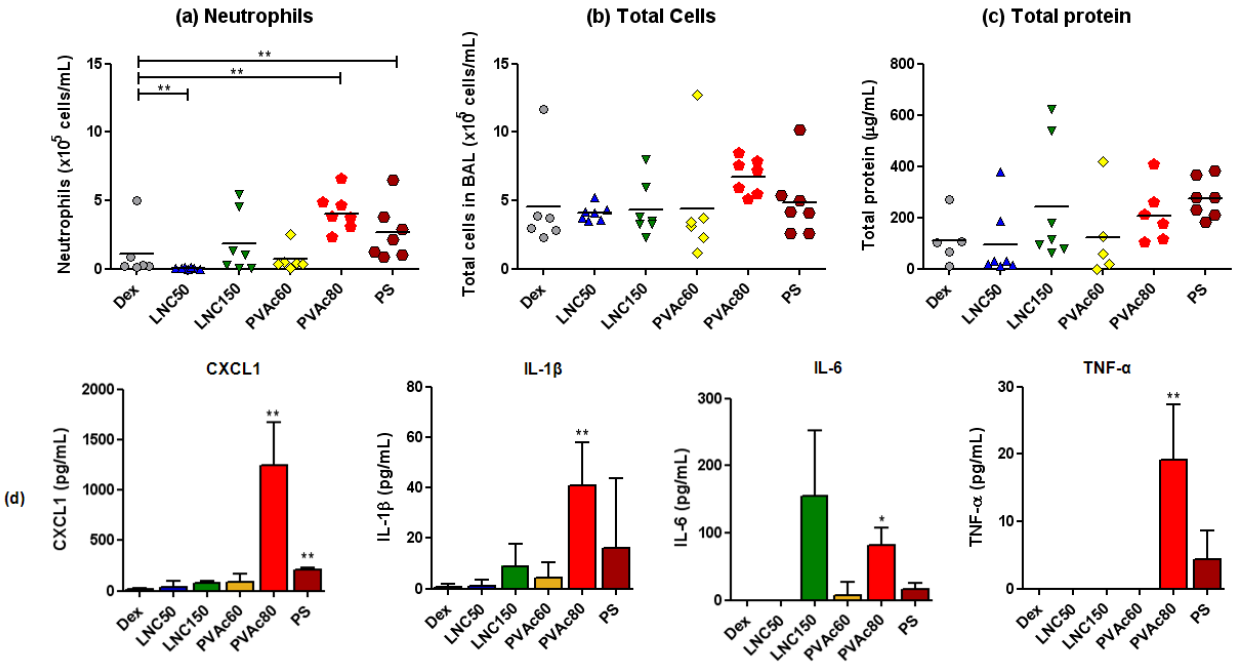
(a) Neutrophils
Neutrophils (x10^5 cells/mL)
(b) Total Cells
Total cells in BAL (x10^5 cells/mL)
(c) Total protein
Total protein (µg/mL)
Dex
LNC50
LNC150
PVAc60
PVAc80
PS
(d)
CXCL1
CXCL1 (pg/mL)
IL-1β
IL-1β (pg/mL)
IL-6
IL-6 (pg/mL)
TNF-α
TNF-α (pg/mL)

Figure 3

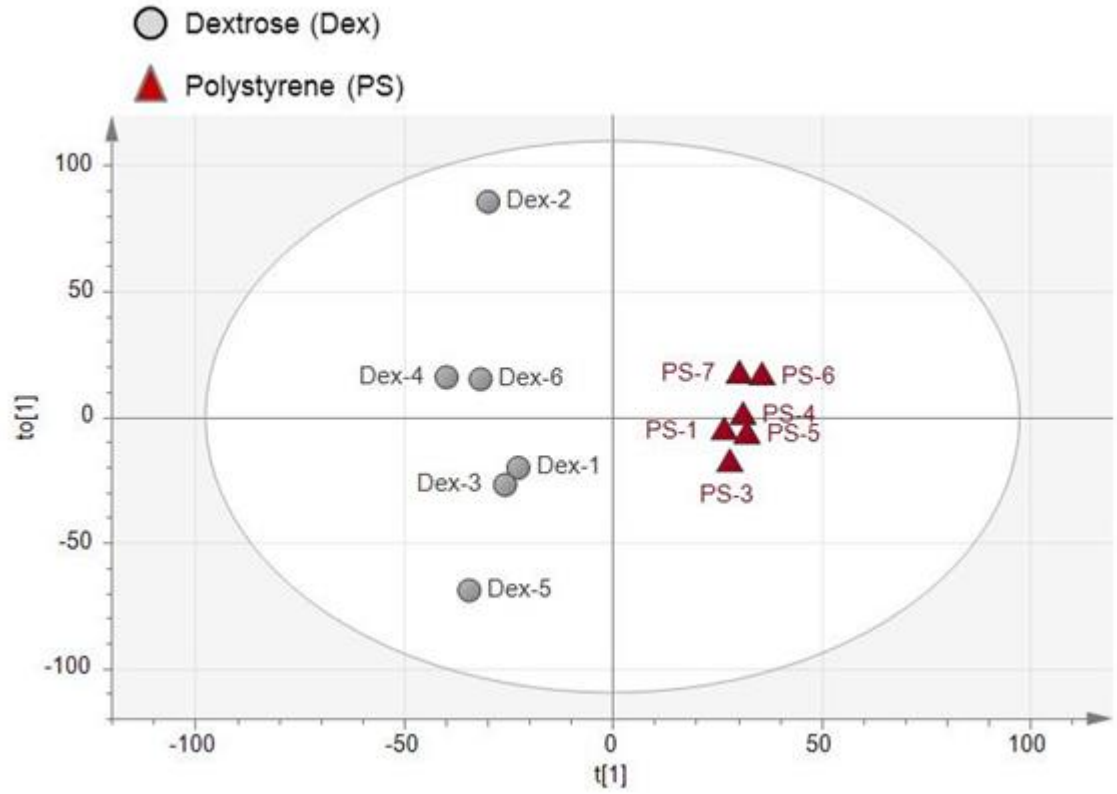
Dextrose (Dex)
Polystyrene (PS)
100
50
0
-50
-100
to[1]
-100
-50
0
50
100
t[1]
Dex-2
Dex-4
Dex-6
Dex-3
Dex-1
Dex-5
PS-7
PS-6
PS-4
PS-1
PS-5
PS-3

Figure 4

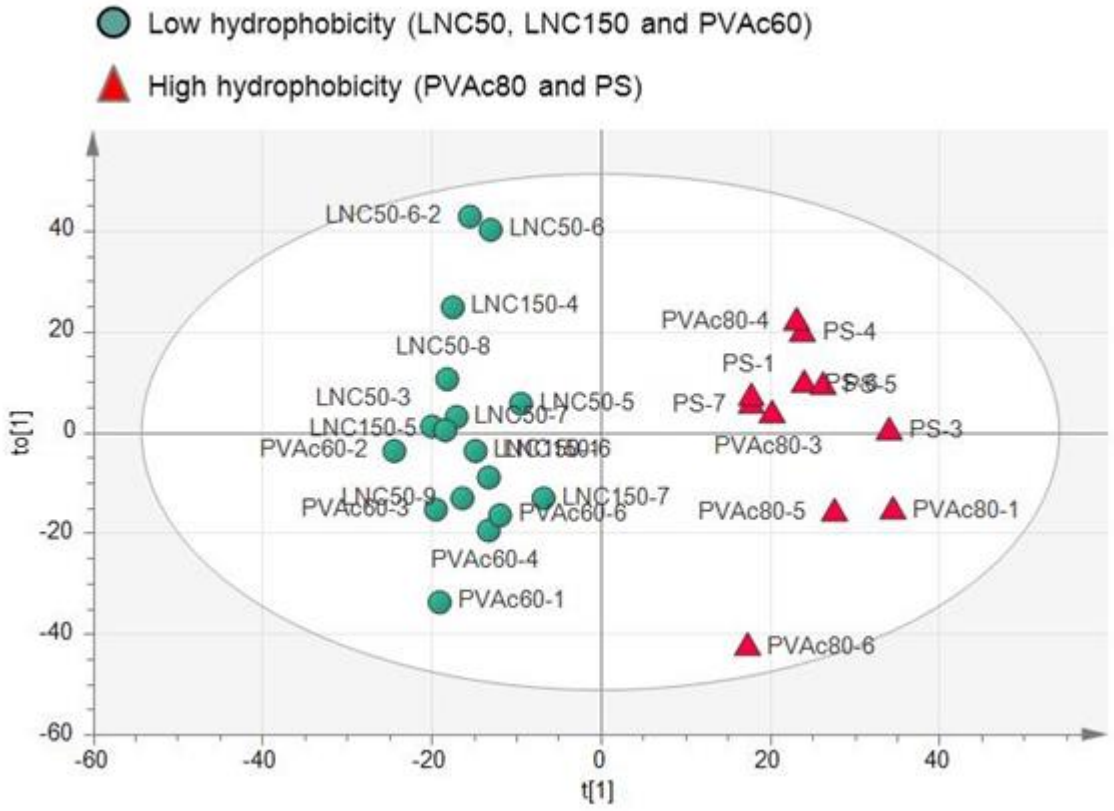
Low hydrophobicity (LNC50, LNC150 and PVAc60)
High hydrophobicity (PVAc80 and PS)
LNC50-6-2
LNC50-6
LNC150-4
LNC50-8
LNC50-3
LNC50-5
LNC50-7
LNC150-5
PVAc60-2
LNC150-6
LNC50-9
PVAc60-3
LNC150-7
PVAc60-6
PVAc60-4
PVAc60-1
PVAc80-4
PS-4
PS-1
PS-7
PS-3
PVAc80-3
PVAc80-5
PVAc80-1
PVAc80-6
to[1]
t[1]
40
20
0
-20
-40
-60
-60
-40
-20
0
20
40

Figure 5

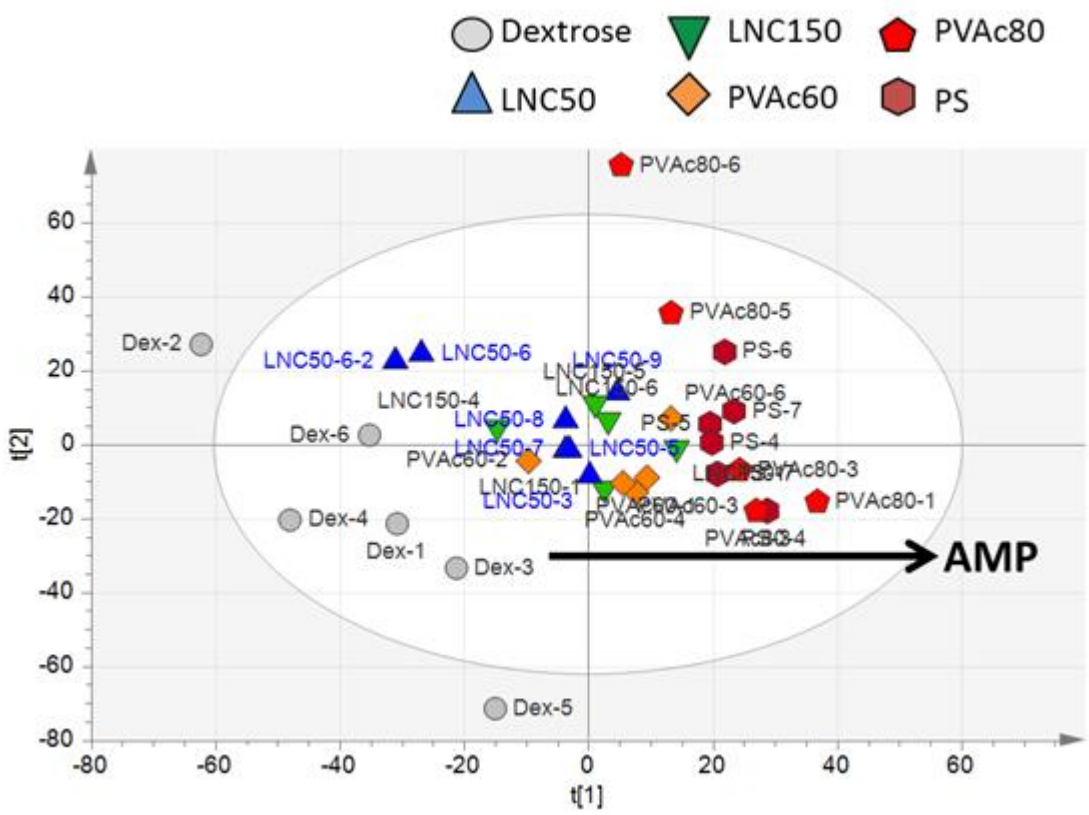
Dextrose
LNC150
PVAc80
LNC50
PVAc60
PS
PVAc80-6
PVAc80-5
PS-6
Dex-2
LNC50-6-2
LNC50-6
LNC50-9
PVAc60-6
PS-7
LNC150-4
LNC50-8
Dex-6
PS-4
LNC50-7
LNC50-5
PVAc60-2
PVAc80-3
LNC150-1
LNC50-3
PVAc80-1
Dex-4
PVAc60-4
Dex-1
Dex-3
AMP
Dex-5
t[1]
t[2]
60
40
20
0
-20
-40
-60
-80

Figure 6

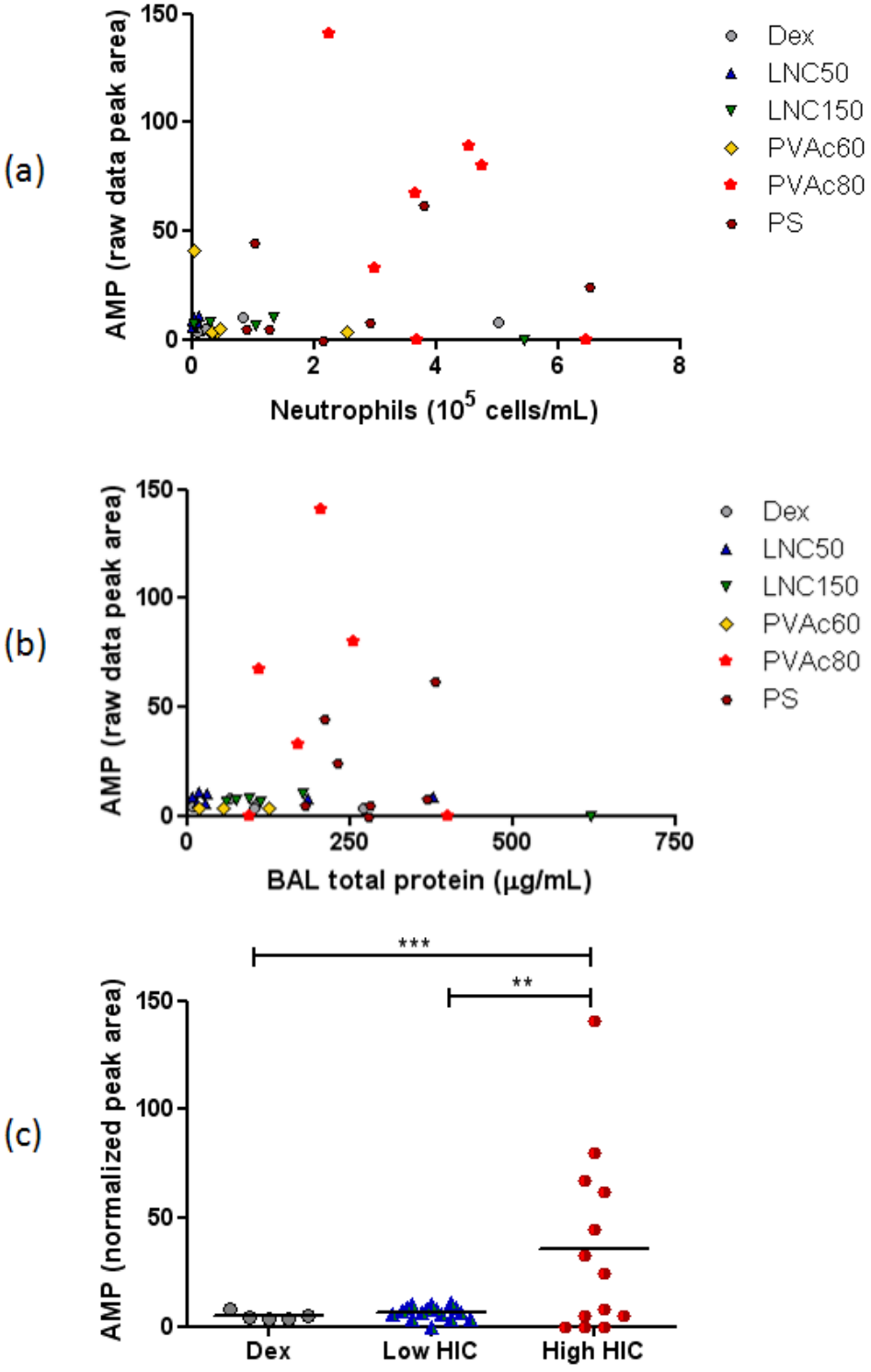
(a)
AMP (raw data peak area)
150
100
50
0
0
2
4
6
8
Neutrophils (10^5 cells/mL)
Dex
LNC50
LNC150
PVAc60
PVAc80
PS
(b)
AMP (raw data peak area)
150
100
50
0
0
250
500
750
BAL total protein (µg/mL)
Dex
LNC50
LNC150
PVAc60
PVAc80
PS
(c)
AMP (normalized peak area)
***
**
150
100
50
0
Dex
Low HIC
High HIC

Figure 7

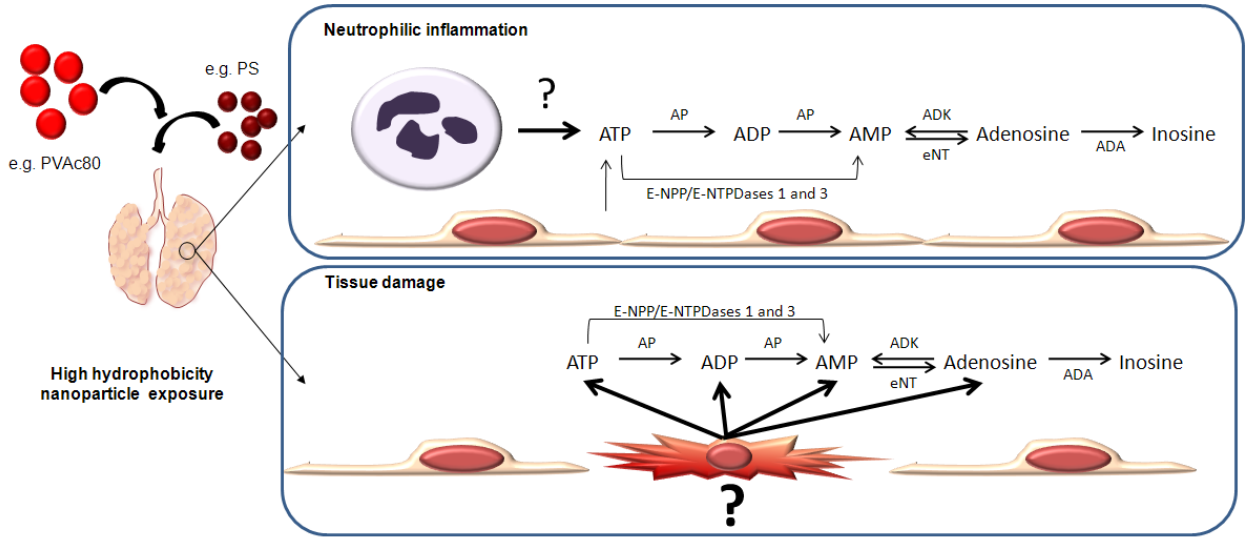
e.g. PS
e.g. PVAc80
High hydrophobicity nanoparticle exposure
Neutrophilic inflammation
?
ATP
AP
ADP
AP
AMP
ADK
eNT
Adenosine
ADA
Inosine
E-NPP/E-NTPDases 1 and 3
Tissue damage
E-NPP/E-NTPDases 1 and 3
ATP
AP
ADP
AP
AMP
ADK
eNT
Adenosine
ADA
Inosine
?

Figure S1

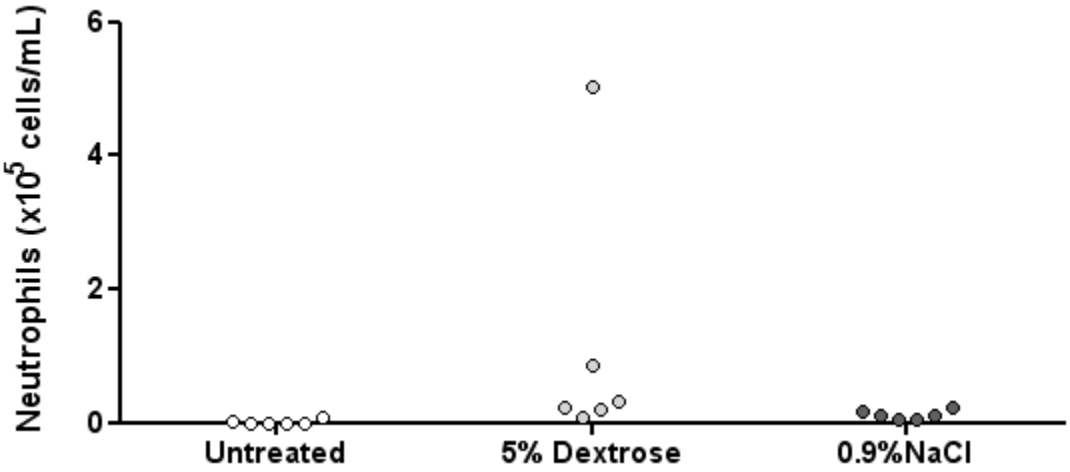


Figure S2

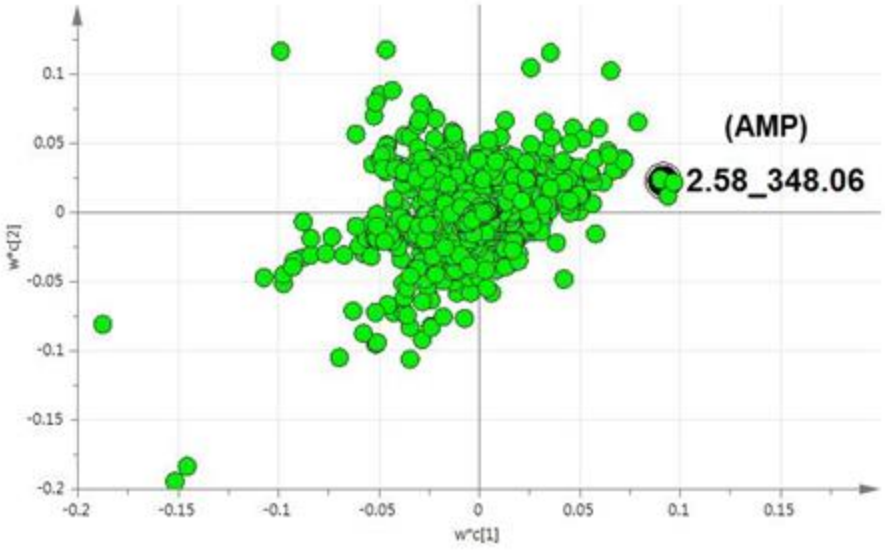

Figure S3

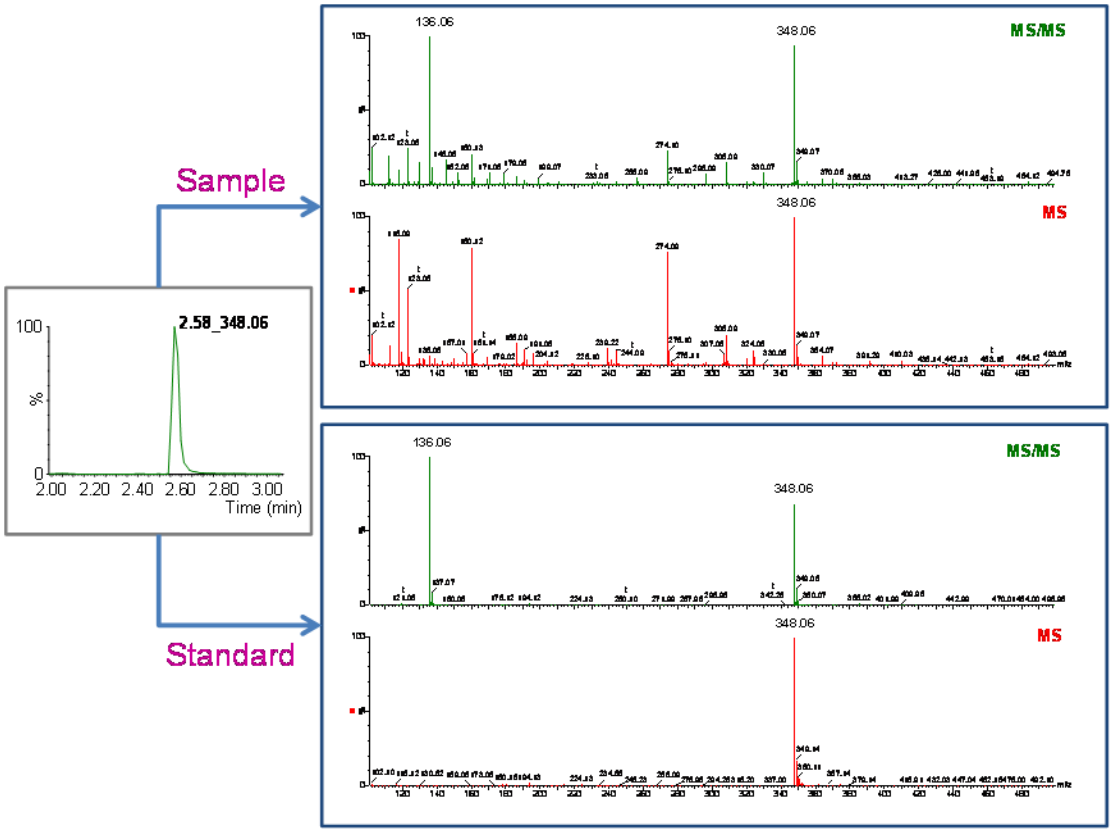
Sample
2.58_348.06
100
%
0
2.00 2.20 2.40 2.60 2.80 3.00
Time (min)
Standard
136.06
348.06
MS/MS
MS
136.06
348.06
MS/MS
MS